Selective Catalytic Reduction of Nitric Oxide with Propylene over Fe/Beta Catalysts Under Lean-Burn Conditions

Hao Zhou [1],* [ID]**, Mengyao Ge [1], Huishuang Zhao [1], Shiguo Wu [1], Mengyu Li [1] and Yaxin Su [2]**

[1] Changzhou Institute of Engineering Technology, Changzhou 213164, China; gmy1615593083@hotmail.com (M.G.); hszhao@czie.edu.cn (H.Z.); sgwu@czie.edu.cn (S.W.); lmyu08@hotmail.com (M.L.)

[2] School of Environmental Science and Engineering, Donghua University, Shanghai 201620, China; suyx@dhu.edu.cn

* Correspondence: hzhou@czie.edu.cn; Tel./Fax: +86-519-8633-2216

Abstract: Fe/Beta catalysts were used for the selective catalytic reduction of nitric oxide with propylene (C_3H_6-SCR) under lean-burn conditions, which were prepared by liquid ion-exchange (LIE), solid-state ion-exchange (SIE), and incipient wet-impregnation (IWI) methods. The iron species on Fe/Beta were characterized and identified by a combination of several characterization techniques. The results showed preparation methods had a significant influence on the composition and distribution of iron species, LIE method inclined to produce more isolated Fe^{3+} ions at ion-exchanged sites than IWI and SIE method. C_3H_6-SCR activity tests demonstrated Fe/Beta(LIE) possessed remarkable catalytic activity and N_2 selectivity at temperature 300–450 °C. Kinetic studies of C_3H_6-SCR reaction suggested that isolated Fe^{3+} species were more active for NO reduction, whereas Fe_2O_3 nanoparticles enhanced the hydrocarbon combustion in excess of oxygen. According to the results of in situ DRIFTS, more isolated Fe^{3+} sites on Fe/Beta(LIE) would promote the formation of the key intermediates, i.e., NO_2 adspecies and formate species, then led to the superior C_3H_6-SCR activity. The slight decrease of SCR activity after hydrothermal aging of Fe/Beta(LIE) catalyst might be due to the migration of isolated Fe^{3+} ions into oligomeric clusters and/or Fe_2O_3 nanoparticles.

Keywords: NO; SCR; C_3H_6; Fe/Beta; iron species

1. Introduction

Nitric oxides (NO_x) from combustion exhaust gas are the major air pollutants drive to the formation of photochemical smog and haze [1,2]. Up to now, the removal of NO_x in the exhaust of diesel engine under lean-burn conditions is still a significant challenge. Selective catalytic reduction of NO_x by hydrocarbons (HC-SCR) is a promising technology for reducing NO_x, which can achieve the elimination of both hydrocarbons and nitric oxides in pollution source at the same time [3]. Transition metal (e.g., Cu, Fe) modified zeolites exhibit remarkable catalytic activity in the HC-SCR process, many studies have been conducted on zeolite structure, metals nature and preparation methods of zeolite catalysts [4–6]. However, the poor hydrothermal stability still limits their practical application [7,8].

Recently, zeolites with Chabazite (CHA) structure, such as SSZ-13 [9,10] and SAPO-34 [11,12], have received much attention due to their outstanding hydrothermal durability and activity in the NH_3-SCR. However, for the HC-SCR reaction, the pore radius of CHA structure (3.8 Å) may be a little smaller for hydrocarbon molecules (e.g., C_3H_8, C_3H_6) through the zeolite channels. Then our work will focus on the metal nature and preparation method of large or medium pore zeolites catalysts. Fe-based zeolites (e.g., Fe/ZSM-5 and Fe/Beta) are more attractive for HC-SCR because of their appropriate

activity at high temperature and better hydrothermal stability [13]. Chen et al. [4] first prepared Fe/ZSM-5 catalysts using the sublimation method for SCR of NO by iso-butane, which exhibited durable activity and high selectivity in the presence of water vapor. Janas et al. [5] reported that FeSiBEA catalyst with low iron content prepared in acidic conditions are active for NO reduction with C_2 reducing agents. Pan et al. [6] compared the support effects on NO_x adsorption and reduction by propylene over a series of Fe/zeolites catalysts, and found that catalytic activity decreases following the order: Fe/Beta > Fe/FER > Fe/ZSM-5 > Fe/MOR at high temperatures (>300 °C). Moreover, Fe/Beta catalysts are more stable against hydrothermal aging than Fe/ZSM-5 due to the difference in the zeolite structures [14].

In general, zeolite-based catalysts are prepared using liquid-phase or solid-state ion-exchange, wet impregnation, and chemical vapor deposition, by which Fe species are introduced into parent zeolite. Fe/zeolite with controllable iron loading can be obtained using wet impregnation, but the zeolite pores are easily blocked by the agglomeration of the Fe species. Fe/zeolite catalyst prepared by the ion-exchange usually exhibits higher activity, however, the activity is also dependent on the exchange level. Furthermore, the complex coexistence of extra-framework Fe species are usually observed in Fe/zeolite catalysts prepared by different methods [15–17]. These Fe species may be present as: (i) isolated and/or binuclear ferric ions anchored to the zeolite framework; (ii) oligomeric clusters formed inside and/or outside the pores; (iii) Fe_2O_3 nanoparticles on the external surface of the zeolite. For NH_3-SCR, previous studies [17,18] had shown isolated iron ions and/or oligomeric Fe_xO_y clusters may be the favorable active sites in Fe/ZSM-5 catalysts. Zhang et al. [19] studied the selective oxidation of methane over FeO_x/SBA-15, and proposed isolated ferric ions as the active sites for the selective oxidation of CH_4 to HCHO, whereas Fe_xO_y clusters are less active and Fe_2O_3 nanoparticles mainly contribute the complete oxidation of CH_4. To best of our knowledge, there has been no systematic analysis and comparison of the correlation of the Fe species and HC-SCR performance over Fe/Beta catalysts.

In this work, Fe/Beta catalysts were prepared by different methods used for SCR of NO by C_3H_6 under lean-burn conditions. To identify and quantify active Fe species in C_3H_6-SCR of iron species, a combination of characterization techniques was applied, such as X-ray diffraction (XRD), high-resolution transmission electron microscope (HRTEM), X-ray photoelectron spectra (XPS) temperature-programmed reduction with hydrogen (H_2-TPR), UV-vis diffuse reflectance spectra (DRS), and in situ diffuse reflectance infrared Fourier transform spectroscopy (DRIFTS). Especially, the evolution of iron species after the hydrothermal aging and their roles in C_3H_6-SCR were also discussed.

2. Results

2.1. Physical Properties

The N_2 adsorption–desorption isotherms of Fe/Beta catalysts prepared by different methods alone with H-Beta support are shown in Figure 1. The isotherms of Fe/Beta samples were similar to H-Beta suggested that the incorporation of Fe species with low content exerted little influence on the textural properties of parent material. In addition, the BET results and Fe loading of samples are summarized in Table 1. The ICP-AES analysis showed that Fe/Beta catalysts prepared by three methods had almost the same Fe loading (about 1.5 wt.%). Compared to parent H-Beta, Fe/Beta sample prepared by LIE method had a slight decrease in the specific surface area (from 519.9 to 512.1 m^2/g). However, the Fe/Beta prepared by IWI and SIE methods showed the obvious decrease of specific surface area (from 519.9 to 480.5 and 486.5 m^2/g, respectively).

In general, Fe/zeolite prepared by wet impregnation could easily cause the aggregation of iron species and partially blocked some zeolite channels [20]. Therefore, it could be assumed that the ferric ions at ion-exchange sites, which might be the main product with LIE method, would little affect the textural properties of Beta zeolite. On the contrary, other iron species (e.g., iron oxide nanoparticles)

might be the by-products with IWI and SIE methods, resulting in the decrease of surface area and pore volume of Fe/Beta catalysts.
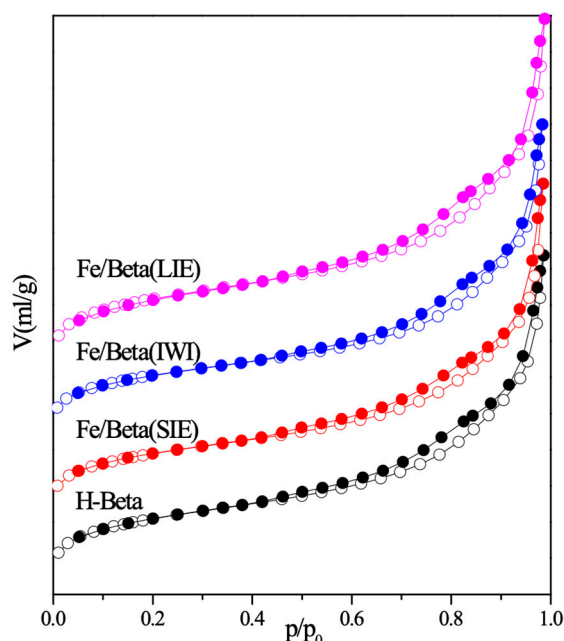

Figure 1. N_2 adsorption–desorption isotherms of H-Beta and Fe/Beta catalysts.

Table 1. Properties of Fe/Beta catalysts prepared by different methods. LIE: liquid ion-exchange; IWI: incipient wet-impregnation; SIE: solid-state ion-exchange.

Sample	Specific Surface Area (m²/g)	Pore Volume (mL/g)	Fe Loading [a] (mg/g)
H-Beta	519.9	0.517	-
Fe/Beta(LIE)	512.1	0.541	13.87
Fe/Beta(IWI)	480.5	0.495	15.70
Fe/Beta(SIE)	486.5	0.506	13.40

[a] Determined by inductively coupled plasma (ICP) analysis.

2.2. Structural Characteristics

To further investigate the influence of preparation method on iron species of Fe/Beta zeolite, the XRD patterns of different Fe/Beta catalysts alone with H-Beta support were tested and depicted in Figure 2. It shows that Beta zeolite diffraction peaks (2θ = 7.7°, 21.6°, 22.5°, 25.5°, 29.7°, 33.6°, and 43.9°) mainly appeared on all Fe/Beta catalysts in Figure 2a, indicated that the introduction of iron species did not destroy the parent zeolite structure. The results were consistent with the N_2 adsorption/desorption results. In Figure 2b, the 2θ region between 31 and 36° was enlarged to observe the characteristic peaks of the Fe_2O_3 phase (JCPDS file No. 79–1741). Although three Fe/Beta samples had almost the same Fe loading (about 1.5 wt.%), the diffraction peak at 33.2° assigned to Fe_2O_3 only appeared on Fe/Beta(SIE) sample. Fe/Beta(LIE) and Fe/Beta(IWI) samples did not show diffraction peaks for the bulk Fe_2O_3, suggesting that iron species were dispersed well or mainly migrated to the ion-exchange sites on these samples. It should be noted that the characteristic peaks at about 33.4° appeared on H-Beta and Fe/Beta samples, which belong to the Beta zeolite diffraction peaks. The characteristic diffraction peak assigned to Fe_2O_3 phase only appeared on Fe/Beta(SIE) sample, which illustrated the Fe_2O_3 nanoparticles were not the dominant iron species, especially when preparing Fe/Beta catalyst with low iron content. These observations imply that the preparation method would lead to some differences of iron species on the Fe/Beta catalysts.
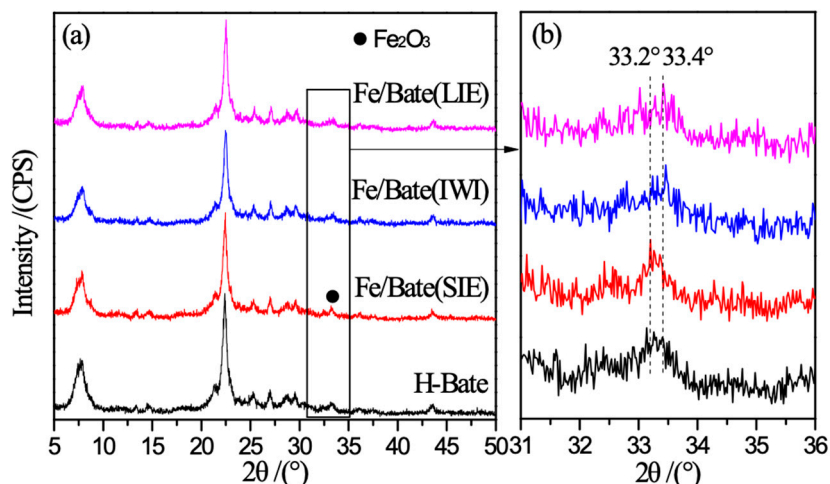
Figure 2. XRD diffractograms of H-Beta and Fe/Beta catalysts, (**a**) a wide scan in the 2θ region of 5–50° and (**b**) an enlarged view in the 2θ region of 31–36°.

2.3. Morphologies

Through the characterization of N_2 adsorption/desorption and XRD, it is not clear whether iron species was incorporated into the framework or it was just dispersed well over the zeolite surface. This needs to be confirmed by means of certain characterization methods. Then the morphologies of Fe/Beta samples were observed by TEM, as shown in Figure 3. It is seen that iron-containing crystalline species (e.g., bulk Fe_2O_3) could not be observed on the surface of Beta support in all samples. In fact, three Fe/Beta samples appeared to be more similar to pure Beta zeolite (not shown). Although the TEM result could not be the direct evidence of the types of iron species, it strongly supported that there was no bulk Fe_2O_3 species existed in Fe/Beta in this case.
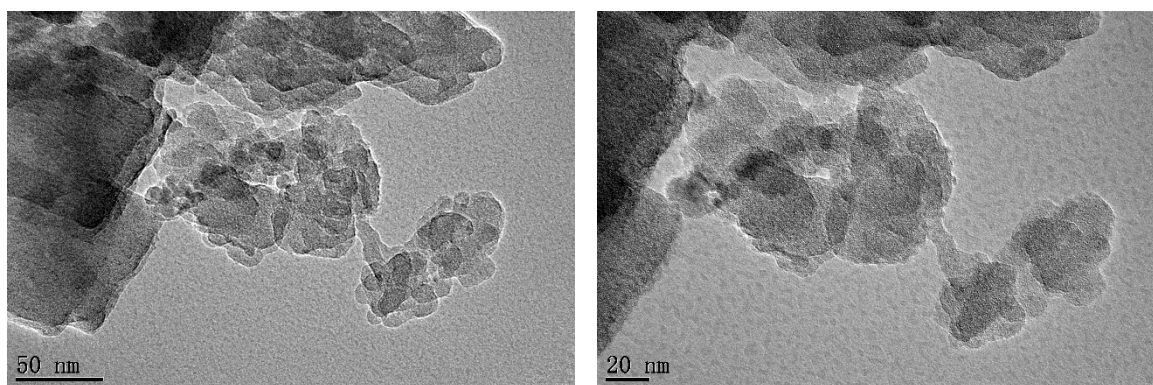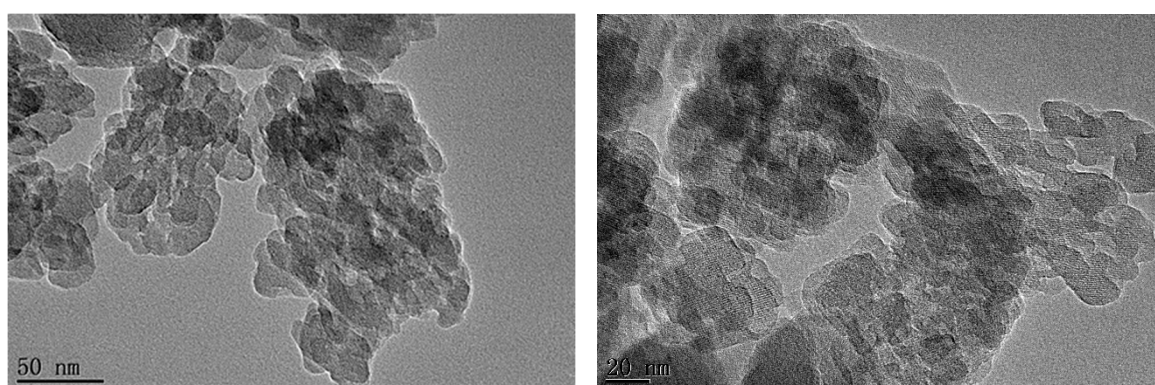

(**a**) Fe/Beta(LIE)

Figure 3. *Cont.*
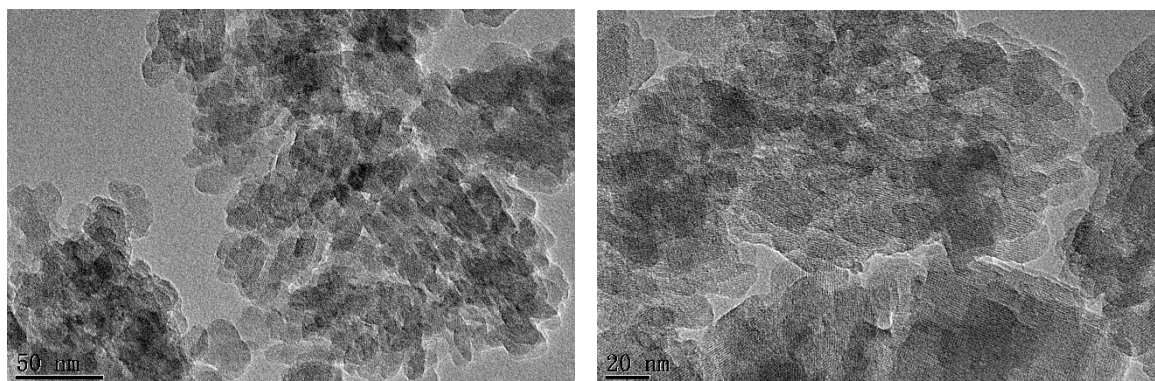
(**b**) Fe/Beta(IWI)

(**c**) Fe/Beta(SIE)

Figure 3. TEM images of Fe/Beta catalysts.

2.4. XPS

XPS analysis was carried out to identify the chemical state of surface iron species. The Fe 2p spectra of Fe/Beta catalysts are shown in Figure S1. The low resolution of Fe 2p spectra is probably due to the low iron content on the surface of Fe/Beta catalysts. It is seen that all Fe/Beta catalysts exhibited two peaks of Fe 2P spectra, the first at 711.3 eV for the Fe 2p3/2 and the second at 725.3 eV for the Fe 2p1/2, with a satellite peak located at 718.9 eV. The binding energies of these peaks can be ascribed to Fe^{3+} ions in the literatures [21,22]. The results imply that iron species on all samples surface primarily existed in the +3 valence state. Among Fe/Beta catalysts prepared by different methods, the highest intensity of peaks assigned to Fe^{3+} could be observed on Fe/Beta(LIE) sample. Considering its excellent C_3H_6-SCR performance, it is considered that the higher amount of Fe^{3+} species will facilitate NO reaction with C_3H_6.

2.5. H_2-TPR

Usually the reduction properties of metal species is closely related with their chemical environment, then the H_2-TPR technique was carried out to speculate iron species on Fe/Beta catalysts. The TPR profiles of different Fe/Beta samples and a comparison with Fe_2O_3 sample (analytically pure, Sinopharm) are showed in Figure 4. As expected, the profile of Fe_2O_3 exhibited a low-temperature peak at 455 °C and a high-temperature peak centered at about 750 °C, which typically attributed to the reduction sequence as $Fe_2O_3 \rightarrow Fe_3O_4 \rightarrow FeO \rightarrow Fe$ [23,24]. Different from the TPR profile of Fe_2O_3, the main reduction peaks of all Fe/Beta samples appeared above 600 °C, which were obvious higher than that of Fe_2O_3. According to our previous study [2,25], the TPR peaks of iron supported metal oxides (e.g., Al_2O_3, TiO_2, and SiO_2) at temperature below 500 °C correspond to the reduction of Fe^{3+} to Fe^{2+}

in nanoparticles, as well as the reduction of Fe_2O_3 to Fe_3O_4, which indicated the presence of crystalline iron oxide phases. The difficulty in reducing the iron species implied that the chemical environment of the iron species of Fe/Beta was different from that of supported metal oxides. We conclude the crystalline phases of Fe_2O_3 were not the main iron species on Fe/Beta samples due to the reduction attributed to iron oxide species did not occur in the H_2-TPR. Wei et al. [26] had also investigated the reduction properties of Fe containing SAPO-34 catalysts, and found that the supported Fe species of impregnated FeAPSO-34 began to reduce at temperature above 300 °C, while no iron species reduction occurred even until 900 °C for synthesized FeAPSO-34.
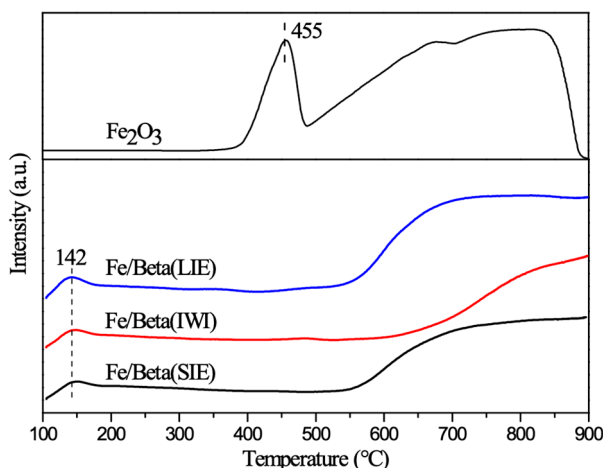

Figure 4. Temperature-programmed reduction with hydrogen (H_2-TPR) profiles of Fe_2O_3 and Fe/Beta catalysts.

Notice that all Fe/Beta samples presented a weak reduction peak at 142 °C, which was much lower than that of ferric oxide. According to the literature [27,28], there may be three different sites for isolated metal ions located in BEA zeolites: the straight channel (α site), a planar deformed six-member ring of the hexagonal cage (β site), and the hexagonal cage (γ site). When the iron species are introduced into the zeolites by liquid ion-exchange, the predominant type of the ferric ions is located in the β site, and a minor amount of ferric ions anchored to α and γ site are formed at Fe/Al >0.1. Moreover, it was found that metal ions in α site are most easily reduced, while ions in γ site are the most difficult reduced site. Ma et al. [20] had also reported the similar reduction peak appeared in Fe/Beta(LIE) samples with low iron content and suggested that such iron species are most likely isolated Fe^{3+} in α site. Based on the above analysis, the main Fe species in Fe/Beta samples with low Fe content were isolated Fe^{3+} ions located in zeolites. The more easily reduced iron species might be related to isolated Fe^{3+} in α site, while much more stabilized isolated Fe^{3+} in β site would be dominant on Fe/Beta samples.

2.6. UV-Vis

UV-vis diffuse reflectance spectra was further applied to characterize Fe species on these Fe/Beta catalysts, and the results are displayed in Figure 5. It is obvious that there was no distinct characteristic bands over H-Beta support, then the bands of Fe/Beta were attributed to Fe-O charge-transfer of different iron species. Schwidder et al. [29] and Feng et al. [30] assigned the bands below 290 nm to isolated Fe^{3+} in tetrahedral and octahedral coordination, the bands in the range of 300–400 nm to oligomeric Fe_xO_y clusters, and the bands above 400 nm to Fe_2O_3 nanoparticles on the external surface of the zeolite. The UV-vis spectra of Fe_2O_3 (as shown in Figure S2) also showed that the primary bands appeared above 400 nm, which could be attributed to Fe_2O_3 crystallites species. To obtain the detailed information of Fe species, the UV-vis spectra was de-convoluted into several sub-bands by Gaussian

method and the results are shown in Figure S3. Moreover, the semi-quantitative analysis of different Fe species by the area ratios of the sub-bands was summarized in Figure 6.
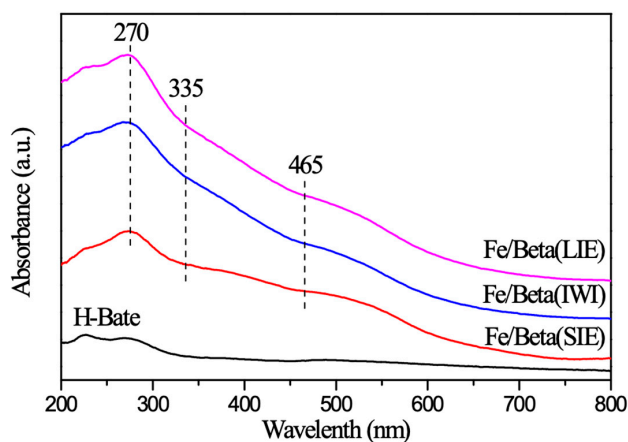

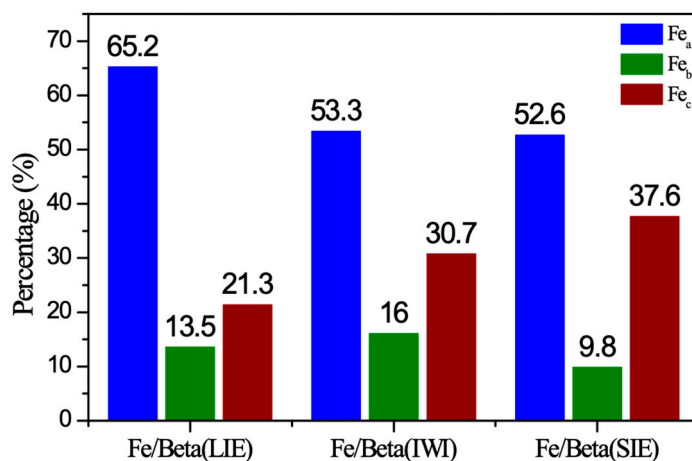**Figure 5.** UV-vis spectra of H-Beta and Fe/Beta catalysts.

Figure 6. Percentage of various Fe species over Fe/Beta catalysts prepared by different methods. (**a**) Isolated Fe^{3+} in tetrahedral and octahedral coordination, (**b**) Oligomeric Fe_xO_y clusters, (**c**) Fe_2O_3 nanoparticles.

Obviously, the distribution of three iron species (e.g., isolated Fe^{3+}, oligomeric Fe_xO_y clusters, and iron oxide nanoparticles) significantly depended on preparation methods. It can be seen that isolated Fe^{3+} ions located at ion-exchanged sites were the main species (more than 50%) on all Fe/Beta samples. The LIE sample showed the strongest characteristic peak (as shown in Figure S3 and Figure 5) around 270 nm, which indicated the formation of high dispersion Fe^{3+} ions with H-Beta interface. The concentration of isolated Fe^{3+} ions could be observed: Fe/beta(LIE) > Fe/beta(IWI) > Fe/beta(SIE). On the contrary, the concentration of Fe_2O_3 nanoparticles followed the order: Fe/beta(SIE) > Fe/beta(IWI) > Fe/beta(LIE). There were more Fe_2O_3 nanoparticles (more than 30%) on the surface of SIE and IMI samples. These results agree well with the BET and XRD results, indicated SIE and IMI methods inclined to produce more iron oxide nanoparticles. However, the concentration of oligomeric Fe_xO_y clusters on three Fe/Beta samples was relatively low (less than 16%). Gao et al. [31] reported that two main Cu species present on Cu/SAPO-34 catalysts prepared by SIE method, and found that isolated Cu^{2+} ions are highly active and selective in NH_3-SCR, while CuO particles mainly contribute to the non-selective oxidation of NH_3 above 350 °C. The role of the different iron species in C_3H_6-SCR reaction will be further discussed later with the results of catalytic activity and in situ DRIFTS studies.

2.7. C3H6-SCR Performance

The C$_3$H$_6$-SCR catalytic behavior of Fe/Beta catalysts were examined in excess of oxygen, and the results are displayed in Figure 7a. For H-beta sample, the maximum NO conversion was only 30% within the whole temperature region. After the introduction of iron species, the NO reduction efficiency over Fe/Beta catalysts increased significantly at the temperature ranges of 250–450 °C. For Fe/Beta(LIE) sample, the maximum NO conversion reached >90% and N$_2$ selectivity achieved >95% in the range of 300–450 °C. It is found that the C$_3$H$_6$-SCR activity decreased in the following order: Fe/Beta(LIE) > Fe/Beta(IWI) > Fe/Beta(SIE) > H-beta. At nearly the same iron content, Fe/Beta(LIE) catalyst exhibited superior catalytic activity than other catalysts, indicating that the preparation method might lead to the different distribution of iron species, which was an important factor affecting C$_3$H$_6$-SCR activity. Furthermore, Fe/Beta(LIE) catalyst in the present case has shown higher HC-SCR activity than other Fe-based zeolite catalysts reported in the literatures (e.g., Fe/ZSM-5 [15], Fe/MFI [32], Fe/SBA-15 [33]), probably due to the Beta zeolite had better adsorption property of hydrocarbons than other zeolites [34].
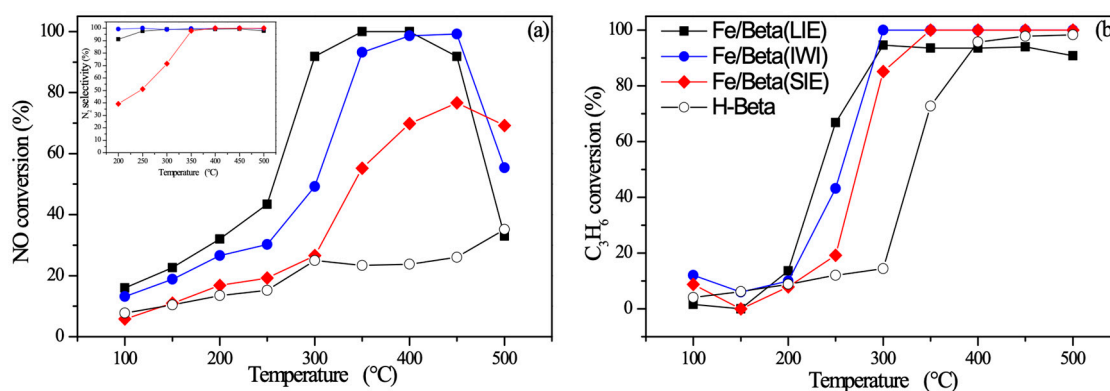

Figure 7. NO conversion and N$_2$ selectivity (**a**) and C$_3$H$_6$ conversion (**b**) over pure H-beta and Fe/Beta catalysts prepared by different methods. The inlet gas mixture consisting of 0.05% NO, 0.05% C$_3$H$_6$, 2% O$_2$ and balance N$_2$. GHSV = 15,000 mLg^{-1}h^{-1}.

The propylene conversions of Fe/Beta catalysts during the reduction of NO were compared in Figure 7b. The highest C$_3$H$_6$ conversion was obtained over Fe/beta(LIE) catalyst when temperature was below 300 °C, and the other Fe/Beta samples exhibited the lower conversion but better than that over H-beta sample, which were consistent with the order of C$_3$H$_6$-SCR activity. When the temperature was above 350 °C, the C$_3$H$_6$ conversion over all Fe/Beta catalysts achieved more than 90%. However, the propylene conversion remained stable with a further increase of temperature, while NO conversion dropped sharply above 450 °C. It implies that the propylene combustion would dominate at high temperatures in C$_3$H$_6$-SCR reaction, resulting in the low selectivity of propylene toward NO reduction.

Taking into account the co-existence of H$_2$O and SO$_2$ in the gas emission form vehicles, it is of particular interest to investigate the influence of H$_2$O/SO$_2$ on DeNO$_x$ performance of Fe/Beta catalysts. The corresponding results concerning the effect of H$_2$O/SO$_2$ on C$_3$H$_6$-SCR activity over Fe/beta(LIE) catalyst are depicted in Figure 8. It is found that similar DeNO$_x$ performance over Fe/beta(LIE) in the presence of 5% H$_2$O could be observed with the active window (e.g., temperature for 50% conversion) shifting a little to lower temperature. On the other hand, the DeNO$_x$ performance was slightly suppressed below 300 °C and the active window shifted by 50 °C to high temperature in the presence of 0.02% SO$_2$. Furthermore, the coexistence of 5% H$_2$O and 0.02% SO$_2$ led to more serious activity decline when the reaction temperature was below 350 °C. However, Fe/beta(LIE) still maintained high activity in the temperature range of 350–450 °C in the coexistence of H$_2$O and SO$_2$. Kucherov et al. [35] proposed that the ferric ions in tetrahedral and distorted tetrahedral sites are responsible for the H$_2$O tolerance of Fe/Zeolite because water vapor do not chemically adsorb on

those ferric ions above 200 °C. The above results suggest that Fe/beta(LIE) catalysts had moderate resistance to SO$_2$ and preferable insensitivity to H$_2$O.
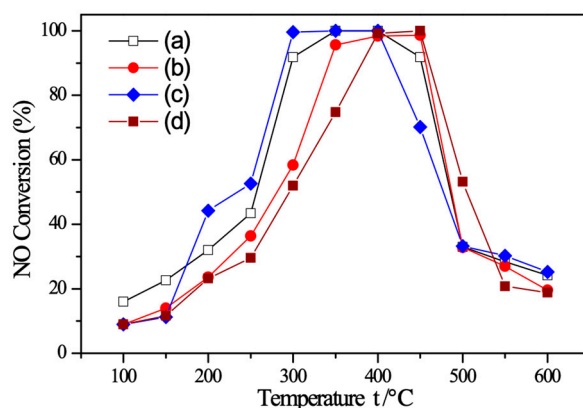

Figure 8. NO conversion over Fe/Beta(LIE) catalysts. Reaction conditions: (**a**) 0.05 NO, 0.05% C$_3$H$_6$, 2% O$_2$, (**b**) 0.05 NO, 0.05% C$_3$H$_6$, 2% O$_2$, 0.02% SO$_2$, (**c**) 0.05 NO, 0.05% C$_3$H$_6$, 2% O$_2$, 5% H$_2$O, and (**d**) 0.05 NO, 0.05% C$_3$H$_6$, 2% O$_2$, 0.02% SO$_2$, 5% H$_2$O.

In addition, hydrothermal durability is a key criterion for SCR catalyst of diesel engine exhaust due to the periodical process of particulate filter regeneration (temperature up to ∼700 °C). In this work, a harsh hydrothermal treatment (700 °C for 24 h in 10 vol.% H$_2$O) was performed on Fe/beta(LIE) catalyst. The C$_3$H$_6$-SCR performance of the fresh and aged Fe/Beta(LIE) samples was compared in Figure 9. When the reaction temperature was below 300 °C, the aged sample displayed the similar catalytic activity to that of the fresh sample. Notably the aged sample still maintained high activity with NO conversion >90% in the temperature range of 300–400 °C. However, the activity of aged sample was obviously less than the fresh sample above 400 °C, indicating that hydrothermal treatment had a slight inhibition effect at high temperatures on C$_3$H$_6$-SCR.
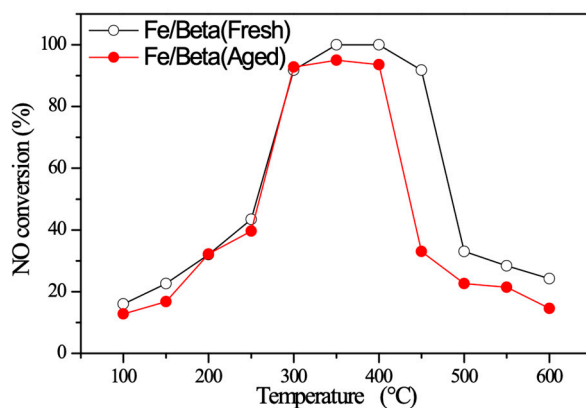

Figure 9. NO conversion over the fresh and aged Fe/Beta(LIE) catalysts. The hydrothermal aging was performed at 700 °C for 24 h in the presence of 10% H$_2$O. Reaction conditions are same as those in Figure 7.

2.8. In Situ DRIFTS

The adsorbed intermediates on the surface of different Fe/Beta catalysts were further investigated by in situ DRIFTS. Figure 10 shows the FT-IR spectra for different exposure times for NO + O$_2$ + C$_3$H$_6$ adsorption at 200 °C.

After NO + O$_2$ co-adsorption for 60 min, the FT-IR spectra of Fe/beta(IWI) and Fe/beta(SIE) samples were quite similar. It can be seen that the bands assigned to bidentate nitrate [36], unidentate nitrate [37], and monodentate nitrite appeared at 1589 cm^{-1}, 1261 cm^{-1}, and 1157 cm^{-1}, respectively.

The weak vibrations located at 3128 and 2952 cm^{-1} could correspond to N_2O_4 adsorption products [38]. Some negative bands around 3682 cm^{-1} were attributed to the vibrations of surface hydroxyl O–H stretching [39]. Among three tested samples, Fe/beta(LIE) exhibited much stronger adsorption toward nitrate species, especially for NO_2 adspecies (nitro or adsorbed NO_2 molecule) on Fe^{3+} sites [40] at 1628 cm^{-1}, which was hardly observed on the surface of Fe/beta(IWI) and Fe/beta(SIE). In addition, the intensity of NO_2 adspecies decreased significantly after evacuation, indicating that a fraction of NO_2 (probably from the oxidation of NO) physically adsorbed on iron sites.
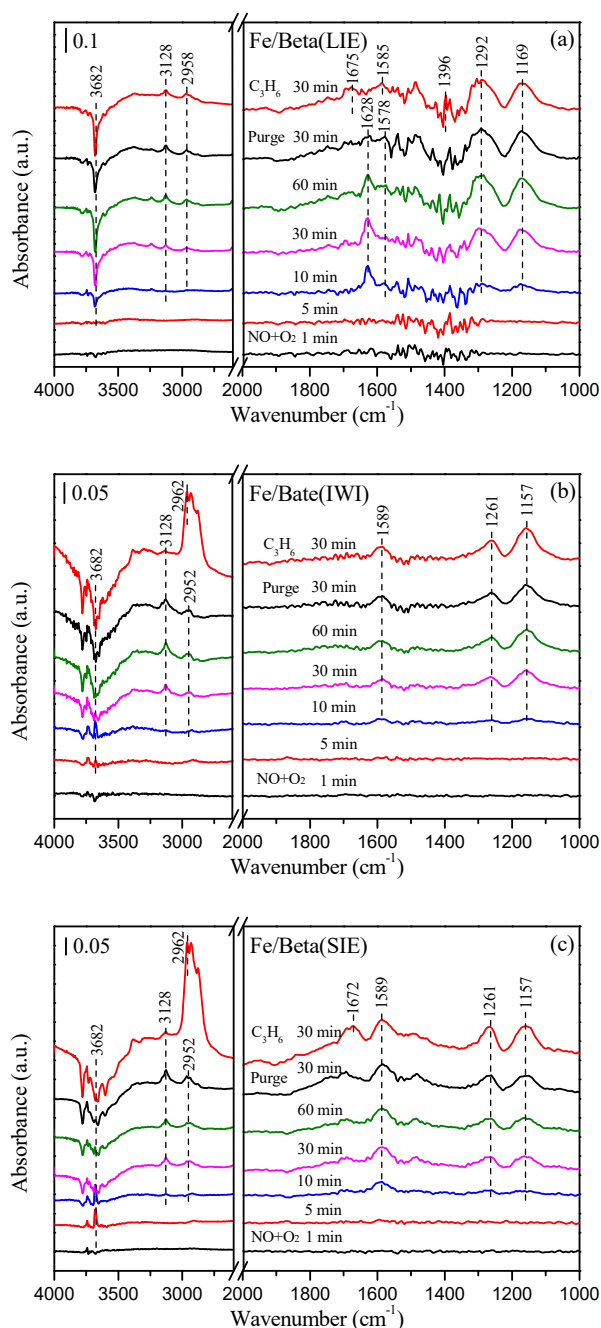

Figure 10. In situ DRIFT spectra measure on Fe/Beta catalysts prepared by different methods (**a**) Fe/Beta(LIE), (**b**) Fe/Beta(IWI) and (**c**) Fe/Beta(SIE) at 200 °C. Treatment: $NO+O_2$ adsorbed 60 min followed by purged in N_2 30 min, then C_3H_6 adsorbed 30 min.

After introduction of C_3H_6 for 30 min over Fe/beta(LIE), some oxidation products from propylene appeared in the 1700–1300 cm^{-1} range. The new band at 1396 cm^{-1} corresponded to formate

species [41], and the band at 1675 cm^{-1} was assigned to amide or organic nitro-compounds [42]. The 1628 cm^{-1} band ascribed to NO_2 adspecies disappeared in company with the intensity of nitrate species decreased gradually. However, Fe/beta(IWI) and Fe/beta(SIE) exhibited weak ability for propylene selective activation, formate species could hardly be perceived in the FT-IR spectra, only the stretching vibration of =C-H assigned to adsorbed propylene [42] appeared around 2962 cm^{-1} during the exposure of C_3H_6 at 200 °C. Liu et al. [43] studied the formation of acetate/formate species by in situ DRIFTS and DFT calculations, which considered as the prerequisite for the generation of –NCO and –CN species. Considering C_3H_6-SCR activity results, we speculate that formate species generated from the selective oxidation of adsorbed propylene would react readily with the adsorbed NO_2/NO_3^- species over Fe/beta(LIE), whereas adsorbed propylene over Fe/beta(IWI) and Fe/beta(SIE) might be less active for NO reduction at low temperatures.

3. Discussion

C_3H_6-SCR activity tests showed that the catalytic behavior of Fe/Beta catalysts prepared by different methods was quite different. At the same support and iron loading, Fe/Beta(LIE) catalyst showed the most active performance for C_3H_6-SCR reaction, which might be related to the maximum relative content of Fe^{3+} ions. In order to further reveal the correlation of the preparation methods on the iron species and C_3H_6-SCR performance, some kinetic studies of the reaction were carried out over Fe/Beta catalysts. According to the percentage of Fe species and NO conversion over Fe/Beta catalysts (Figures 6 and 7), we correlated the content of isolated Fe^{3+} with the NO conversion rate at 200 °C, and the results are showed in Figure 11. It is interesting to see that NO conversion rate increased monotonically with increasing the content of isolated Fe^{3+} species on Fe/Beta. These results implied that the isolated Fe^{3+} ions might be the immediate factor affecting the C_3H_6-SCR activity. Furthermore, we calculated the apparent turnover frequencies (TOF, number of NO molecules converted per Fe per second) of Fe/Beta with total iron, and the TOF function at 200 °C is showed Figure S4. The Fe/Beta(LIE) sample with more isolated Fe^{3+} ions showed a higher frequencies than other samples with the same iron loading, which also indicated isolated Fe^{3+} might be more active for NO reduction.
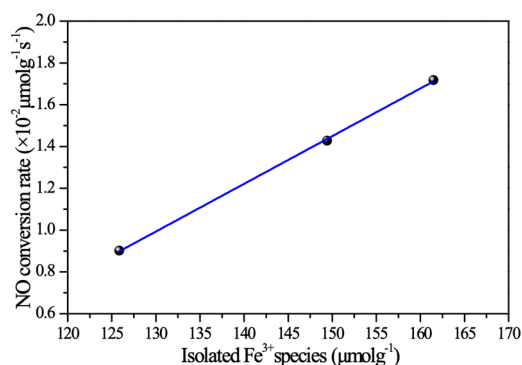

Figure 11. Correlations of the NO conversion rate at 200 °C with the isolated Fe^{3+} content on Fe/Beta catalysts.

From the results of Figure 7, it follows that the SCR reaction was predominant over the Fe/Beta(LIE) catalyst at temperatures below 400 °C but the propylene combustion would prevail at temperatures above 400 °C. Since the hydrocarbon combustion was typically accompanying the HC-SCR reaction and N_2O was hardly observed in the products, there were two main reaction pathways in C_3H_6-SCR over Fe/Beta, which could be represented as:

$$C_3H_6 + 2NO + 3.5O_2 \rightarrow N_2 + 3CO_2 + 3H_2O \tag{1}$$

$$C_3H_6 + 4.5O_2 \rightarrow 3CO_2 + 3H_2O \tag{2}$$
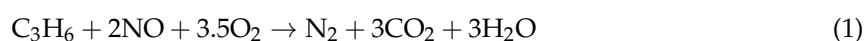
According to our previous work [25,44], Fe_2O_3 nanorods dispersed on the surface of supports play a crucial role for NO reduction while enhance the complete oxidation of hydrocarbon, then a small amount of excess hydrocarbons is required for achieving a satisfactory NO conversion in the presence of oxygen. Fierro et al. [15] reported Fe_xO_y nanoparticles on over-exchanged Fe-ZSM-5 catalysts are not so effective for the HC-SCR reaction but enhance the propane combustion to CO_2. Consequently, the isolated Fe^{3+} species were contributed to the C_3H_6-SCR reaction, Fe_2O_3 nanoparticles were less active for C_3H_6-SCR in presence of oxygen while enhanced the hydrocarbon combustion.

In situ DRIFTS further identified different iron species through the intermediates probably originated from specific iron sites. On the Fe/Beta(LIE) sample, the intensity of adsorbed intermediates (e.g., NO_2 adspecies and formate species) was obviously stronger than that of other samples, which indicated the formation of these intermediates mainly bonded to isolated Fe^{3+} sites. On the contrary, the adsorbed propylene species on Fe/beta(IWI) and Fe/beta(SIE) were much more than Fe/beta(LIE), implied Fe_2O_3 nanoparticles preferred to promote the formation of adsorbed propylene. M. Santhosh Kumar et al. [45] reported that the formation of nitrogen oxide intermediates in higher oxidation states requires the presence of trivalent active Fe sites, which undergo a periodic Fe^{3+}/Fe^{2+} redox cycle. However, Fe_xO_y clusters have a higher oxidizing power than isolated Fe^{3+} sites, then lead to the unselective oxidation of the isobutane reductant. Based on our previous work [25,46], the HC-SCR reaction usually begins with the formation of $NO_2/NO_3{}^-$ and $C_xH_yO_z$ species. Thus more isolated Fe^{3+} sites on Fe/Beta(LIE) would enhance the formation of the key intermediates, i.e., NO_2 adspecies and formate species, then led to the superior C_3H_6-SCR activity.

Moreover, the catalytic activity decreased at high temperatures after hydrothermal treatment (Figure 9), which is another evidence that the distribution of iron species will affect C_3H_6-SCR performance. As can be seen from the XRD profiles (Figure S5), the Beta crystalline phase maintained well even after hydrothermal aging, implying that the inhibition of activity was not related to the deterioration of zeolite framework structure. Compared with the UV-vis spectra with deconvolution for the fresh and aged sample (Figure S6), the intensity of the band below 290 nm decreased while the intensity of the band above 400 nm increased after hydrothermal aging. The relative percentage of isolated Fe^{3+} ions (the species more active for NO reduction) decreased from 65.2% to 51.3%, oligomeric Fe_xO_y clusters (the species may be less active for NO reduction) increased from 13.5% to 20.7%, and Fe_2O_3 nanoparticles (the species more active for hydrocarbon combustion) increased from 21.3% to 28.0%, as shown in Table S1. Kucherov et al. [35] pointed out that isolated Fe^{3+} can migrate out of position and be incorporated into Fe_xO_y clusters during high temperature calcination. Therefore, the slight decrease of catalysis activity at high temperatures after hydrothermal treatment might be due to the migration of isolated Fe^{3+} ions into oligomeric clusters and/or Fe_2O_3 nanoparticles.

On the other hand, the strong acidity of Beta zeolite may be one of important factors for HC-SCR reaction. Then Py-FTIR tests were further performed to investigate the nature of the acid sites on Fe/beta catalysts, and the results are showed in Figure 12. All Fe/Beta samples showed characteristic peaks around 1545, 1490, and 1450 cm^{-1}, corresponding to the pyridine coordinated on Brønsted acid sites, Lewis–Brønsted acid complex, and Lewis acid sites, respectively [47,48]. Table 2 listed the concentration of acid sites on Fe/beta samples calculated according to Beer–Lambert law and the IMEC values. Under desorption conditions at 150 and 300 °C, the strength of Brønsted (229.23 and 197.24 μmol/g) and Lewis acidity (555.66 and 251.65 μmol/g) on Fe/Beta (LIE) sample was almost the lowest in three samples. It is general considered that Brønsted acid sites of zeolite are caused by the bridging hydroxyl protons in the vicinity of the tetrahedrally coordinated lattice-Al atoms. When iron was introduced to H-Beta, Fe^{3+} ion could substitute the H proton of bridging hydroxyls on zeolite, therefore Fe/Beta(LIE) with more isolated Fe^{3+} ions showed weaker acidity compared with Fe/Beta(IWI) and Fe/Beta(SIE) samples. Interestingly, Fe/Beta(LIE) catalyst with weaker acidity exhibited superior catalytic activity, which indicated that too many acid sites might not be necessary for C_3H_6-SCR reaction on Fe/Beta catalysts. The results are in accordance with previous

reports [20,49], which showed that acidity of Fe-zeolite catalyst is not a crucial factor for high SCR activity, but Brønsted acid sites are necessary to bind and disperse the metal ions.
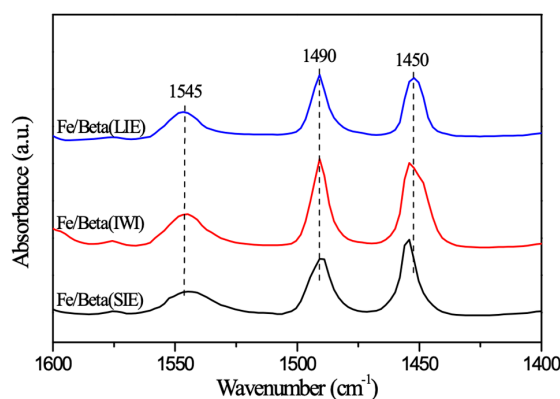

Figure 12. FT-IR spectra of pyridine adsorption at 300 °C on Fe/Beta catalysts.

Table 2. Concentration of surface acid sites of Fe/Beta catalysts.

Sample	150 °C Desorption (μmol/g)		300 °C Desorption (μmol/g)	
	Brønsted Acidity	**Lewis Acidity**	**Brønsted Acidity**	**Lewis Acidity**
Fe/Beta(LIE)	229.23	555.66	197.24	251.65
Fe/Beta(IWI)	335.01	706.06	264.77	515.47
Fe/Beta(SIE)	288.63	631.22	194.10	346.45

4. Materials and Methods

4.1. Catalyst Preparation

Fe/Beta catalysts were prepared by liquid ion-exchange (LIE), solid-state ion-exchange (SIE) and incipient wet-impregnation (IWI) methods. H-Beta (Si/Al$_2$ = 25, Nankai University Catalyst Plant, Tianjin, China) and Fe(NO$_3$)$_3$·9H$_2$O (analytically pure, Sinopharm, Shanghai, China) were used as the parent zeolite and Fe precursor, respectively.

For the LIE method, Fe was introduced into the H-Beta by liquid ion-exchange with Fe(NO$_3$)$_3$ solution (0.1 M, 1 g zeolite/10 mL solution). The slurry was stirred vigorously at room temperature for 24 h. Then the mixture was centrifuged and washed repeatedly with deionized water until the filtrate became neutral, followed by drying at 110 °C for 12 h and calcining at 500 °C in air for 5 h. The process including ion-exchange, centrifugation, rinsing and drying was repeated several times. For the SIE method, Fe was introduced into the H-Beta by solid-state ion-exchange with Fe(NO$_3$)$_3$·9H$_2$O powder (0.11 g iron nitrate/1g zeolite), the mixture of fine milling powders was placed in a flow reactor, heated to 500 °C for 2 h under nitrogen atmosphere. The obtained sample was then dried at 110 °C for 12 h and calcined at 500 °C in air for 5h. For the IWI method, Fe(NO$_3$)$_3$ solution was added dropwise into H-Beta powder to give a 1.5% Fe loading on the catalyst. Then mixture was kept stationary at room temperature for 12 h, following the drying step for 12 h at 110 °C. Finally, the dried sample was calcined at 500 °C in air for 5 h.

The resulting catalysts with the Fe loading of about 1.5 wt.% were denoted as Fe/Beta(LIE), Fe/Beta(SIE), Fe/Beta(IWI), respectively. The hydrothermal treatment of Fe/Beta(LIE) sample was carried out at 700 °C in 10 vol.% H$_2$O for 24 h, and the aged catalyst was designated as Fe/Beta(LIE)-Aged.

4.2. Catalysts Characterizations

The textural property of samples was characterized by adsorption/desorption of N$_2$ at −196 °C using Micromeritics ASAP-2460 apparatus (Norcross, CA, USA). The specific surface area and pore

volume were calculated based on the BET and BJH equation, respectively. High-resolution transmission electron microscopy (HRTEM) was carried out in a JEM-2100F (JEOL, Tokyo, Japan) electron microscope with an accelerating voltage of 100 kV. The iron content in Fe/Beta was measured by inductively coupled plasma-atomic emission (ICP-OES, Agilent 725, Santa Clara, CA, USA).

The powder XRD was performed on a D/max-2550PC diffractometer (Tokyo, Japan) using Cu Kα radiation source (λ = 1.5418 Å). The XRD patterns were collected in the range of 5–80° at a scan rate of 2 °/min. XPS experiments were carried out on a ThermoFisher K-Alpha spectrometer (Waltham, MA, USA) using Al-Kα (1486.6 eV) radiation as the excitation source, the binding energies of Fe 2p, O 1s and Al 2p were referenced to the 284.6 eV C 1s.UV-vis diffuse reflectance spectra measurements were performed on a UV3600 spectrometer equipped with an ultraviolet-visible near-infrared spectrometer (KYOTO, Japan). The detection wavelength range was 190–800 nm (the integrating sphere was 190–2600 nm).

H_2-TPR measurements were performed on an AutoChem II 2920 chemisorption analyzer (Newark, DE, USA). Prior to reduction, the sample (100 mg) was pretreated in He atmosphere at 300 °C for 30 min and then cooled down to 50 °C, and the reduction process was carried out up to 900 °C with a ramp rate of 10 °C/min in a stream of 10 vol.% H_2/Ar.

The acid sites of the catalysts were measured by pyridine adsorption using FT-IR Frontier Infrared Spectrometer (Py-FTIR, Denver, CO, USA). The sample (100 mg) was pretreated at 300 °C in vacuum for 60 min, then cooled down to room temperature and adsorbed by pyridine for 30 min, finally infrared spectra were recorded when pyridine desorption occurred at 150 and 300 °C.

4.3. Catalytic Activity Tests

The activity of Fe/Beta catalysts in the SCR of NO with C_3H_6 was conducted in a quartz tube microreactor, and the schematic diagram and experimental procedures were reported previously [2]. In this study, the reactant gases containing 500 ppm NO, 500 ppm C_3H_6, 2% O_2, 5% H_2O (when needed), 200 ppm SO_2 (when needed), and the balance of N_2 were introduced at a flow rate of 100 mL/min (GHSV = 15,000 mLg^{-1}h^{-1}). The concentrations of C_3H_6, NO, NO_2, N_2O and SO_2 were online measured by FTIR spectroscopy (Thermo Nicolet IS10) and the spectra were collected for a period of 30 min at the aimed temperature. NO conversion and N_2 selectivity were calculated according to the following equations:

$$\text{NO } conversion \text{ (\%)} = \frac{[\text{NO}]_{in} - [\text{NO}]_{out}}{[\text{NO}]_{in}} \times 100\% \tag{3}$$

$$\text{N}_2 \text{ } selectivity \text{ (\%)} = \frac{[\text{NO}]_{in} - [\text{NO}]_{out} - [\text{NO}_2]_{out} - 2[\text{N}_2\text{O}]_{out}}{[\text{NO}]_{in} - [\text{NO}]_{out}} \times 100\% \tag{4}$$

4.4. In Situ DRIFTS Studies

The intermediates on the surface of catalysts during the reaction were investigated by in situ FTIR spectroscopy (Thermo Nicolet IS50), which equipped with an MCT/A detector using DRIFT cell. The scan number was 64 with a resolution of 8 cm^{-1}. Prior to each experiment, Fe/Beta sample (~50 mg) was pretreated in N_2 at 500 °C for 2 h to remove impurities. The gas mixture consisted of 500 ppm NO, 2% O_2 with N_2 as the balance (20 mL/min) was introduced into the reaction cell, then saturated adsorption for 60 min followed by evacuation for 30 min, finally the gas mixture containing 0.1% C_3H_6/N_2 was introduced and a series of time-dependent DRIFT spectra were recorded.

5. Conclusions

In this work, we studied the selective catalytic reduction of NO with C_3H_6 over Fe/Beta catalysts prepared by LIE, SIE, and IWI methods. Combined with the characterization results, isolated Fe^{3+} ions, oligomeric Fe_xO_y clusters and iron oxide nanoparticles coexisted on Fe/Beta catalysts with low iron loading. The preparation methods had a significant influence on the composition and distribution of

iron species, and LIE method inclined to produce more isolated Fe^{3+} ions at ion-exchanged sites than IWI and SIE method.

C_3H_6-SCR activity showed Fe/Beta(LIE) sample exhibited the highest catalytic activity with NO conversion >90% and N_2 selectivity >95% at temperature 300–450 °C, and Fe/Beta(LIE) sample showed the appropriate resistance to SO_2 and H_2O. Kinetic studies of C_3H_6-SCR reaction suggested that isolated Fe^{3+} species were more active for NO reduction, whereas Fe_2O_3 nanoparticles enhanced the hydrocarbon combustion in excess of oxygen. According to the results of in situ DRIFTS, more isolated Fe^{3+} sites on Fe/Beta(LIE) would enhance the formation of the key intermediates, i.e., NO_2 adspecies and formate species, then led to the superior C_3H_6-SCR activity. The slight decrease of catalytic activity at high temperatures after hydrothermal treatment might be due to the migration of isolated Fe^{3+} ions into oligomeric clusters and/or Fe_2O_3 nanoparticles. Furthermore, Py-FTIR tests showed the excessive acid sites were not necessary for C_3H_6-SCR on Fe/Beta catalysts.

Author Contributions: H.Z. (Hao Zhou) and Y.S. designed and administered the experiments. M.G. and M.L. performed experiments. H.Z. (Huishuang Zhao) and S.W. collected and analyzed data. H.Z. (Hao Zhou) wrote the manuscript.

Conflicts of Interest: The authors declare no conflict of interest.

References

1. Liu, Y.; Liu, Z.; Wang, Y.; Yin, Y.; Pan, J.; Zhang, J.; Wang, Q. Simultaneous absorption of SO_2 and NO from flue gas using ultrasound/Fe^{2+}/heat coactivated persulfate system. *J. Hazard. Mater.* **2017**, *342*, 326–334. [CrossRef] [PubMed]

2. Zhou, H.; Ge, M.; Wu, S.; Ye, B.; Su, Y. Iron based monolithic catalysts supported on Al_2O_3, SiO_2, and TiO_2: A comparison for NO reduction with propane. *Fuel* **2018**, *220*, 330–338. [CrossRef]

3. Sánchez-López, P.; Kotolevich, Y.; Miridonov, S.; Chávez-Rivas, F.; Fuentes, S.; Petranovskii, V. Bimetallic AgFe Systems on Mordenite: Effect of Cation Deposition Order in the NO Reduction with C_3H_6/CO. *Catalysts* **2019**, *9*, 58. [CrossRef]

4. Chen, H.Y.; Sachtler, W.M.H. Activity and durability of Fe/ZSM-5 catalysts for lean burn NOx reduction in the presence of water vapor. *Catal. Today* **1998**, *42*, 73–83. [CrossRef]

5. Janas, J.; Rojek, W.; Shishido, T.; Dzwigaj, S. Selective catalytic reduction of NO on single site FeSiBEA zeolite catalyst: Influence of the C_1 and C_2 reducing agents on the catalytic properties. *Appl. Catal. B* **2012**, *123*, 134–140. [CrossRef]

6. Pan, H.; Guo, Y.; Bi, H.T. NO_x adsorption and reduction with C_3H_6 over Fe/zeolite catalysts: Effect of catalyst support. *Chem. Eng. J.* **2015**, *280*, 66–73. [CrossRef]

7. Wang, J.; Zhao, H.; Haller, G.; Li, Y. Recent advances in the selective catalytic reduction of NOx with NH_3 on Cu-Chabazite catalysts. *Appl. Catal. B* **2017**, *202*, 346–354. [CrossRef]

8. Liu, Z.; Ihl Woo, S. Recent advances in catalytic DeNO$_x$ science and technology. *Catal. Rev.* **2006**, *48*, 43–89. [CrossRef]

9. Kwak, J.H.; Tonkyn, R.G.; Kim, D.H.; Szanyi, J.; Peden, C.H.F. Excellent activity and selectivity of Cu-SSZ-13 in the selective catalytic reduction of NOx with NH_3. *J. Catal.* **2010**, *275*, 187–190. [CrossRef]

10. Ren, L.; Zhu, L.; Yang, C.; Chen, Y.; Sun, Q.; Zhang, H.; Li, C.; Nawaz, F.; Meng, X.; Xiao, F.S. Designed copper-amine complex as an efficient template for one-pot synthesis of Cu-SSZ-13 zeolite with excellent activity for selective catalytic reduction of NOx by NH$_3$. *Chem. Commun.* **2011**, *47*, 9789–9791. [CrossRef] [PubMed]

11. Liu, X.; Wu, X.; Weng, D.; Si, Z.; Ran, R. Evolution of copper species on Cu/SAPO-34 SCR catalysts upon hydrothermal aging. *Catal. Today* **2017**, *281*, 596–604. [CrossRef]

12. Andonova, S.; Tamm, S.; Montreuil, C.; Lambert, C.; Olsson, L. The effect of iron loading and hydrothermal aging on one-pot synthesized Fe/SAPO-34 for ammonia SCR. *Appl. Catal. B* **2016**, *180*, 775–787. [CrossRef]

13. Metkar, P.S.; Salazar, N.; Muncrief, R.; Balakotaiah, V.; Harold, M.P. Selective catalytic reduction of NO with NH$_3$ on iron zeolite monolithic catalysts: Steady-state and transient kinetics. *Appl. Catal. B* **2011**, *104*, 110–126. [CrossRef]

14. He, C.; Wang, Y.; Cheng, Y.; Lambert, C.K.; Yang, R.T. Activity, stability and hydrocarbon deactivation of Fe/Beta catalyst for SCR of NO with ammonia. *Appl. Catal. A* **2009**, *368*, 121–126. [CrossRef]

15. Fierro, G.; Moretti, G.; Ferraris, G.; Andreozzi, G.B. A Mössbauer and structural investigation of Fe-ZSM-5 catalysts: Influence of Fe oxide nanoparticles size on the catalytic behaviour for the NO-SCR by C$_3$H$_8$. *Appl. Catal. B* **2011**, *102*, 215–223. [CrossRef]

16. Yuan, E.; Wu, G.; Dai, W.; Guan, N.; Li, L. One-pot construction of Fe/ZSM-5 zeolites for the selective catalytic reduction of nitrogen oxides by ammonia. *Catal. Sci. Technol.* **2017**, *7*, 3036–3044. [CrossRef]

17. Iwasaki, M.; Yamazaki, K.; Banno, K.; Shinjoh, H. Characterization of Fe/ZSM-5 DeNO$_x$ catalysts prepared by different methods: Relationships between active Fe sites and NH$_3$-SCR performance. *J. Catal.* **2008**, *260*, 205–216. [CrossRef]

18. Brandenberger, S.; Kröcher, O.; Tissler, A.; Althoff, R. The determination of the activities of different iron species in Fe-ZSM-5 for SCR of NO by NH$_3$. *Appl. Catal. B* **2010**, *95*, 348–357. [CrossRef]

19. Zhang, Q.; Li, Y.; An, D.; Wang, Y. Catalytic behavior and kinetic features of FeO$_x$ /SBA-15 catalyst for selective oxidation of methane by oxygen. *Appl. Catal. A* **2009**, *356*, 103–111. [CrossRef]

20. Ma, L.; Chang, H.; Yang, S.; Chen, L.; Fu, L.; Li, J. Relations between iron sites and performance of Fe/HBEA catalysts prepared by two different methods for NH$_3$-SCR. *Chem. Eng. J.* **2012**, *209*, 652–660. [CrossRef]

21. Yang, S.; Guo, Y.; Yan, N.; Wu, D.; He, H.; Qu, Z.; Chen, Y.; Zhou, Q.; Jia, J. Nanosized Cation-Deficient Fe-Ti Spinel: A Novel Magnetic Sorbent for Elemental Mercury Capture from Flue Gas. *ACS Appl. Mater. Interfaces* **2011**, *3*, 209–217. [CrossRef] [PubMed]

22. Li, W.; Li, G.; Jin, C.; Liu, X.; Wang, J. One-step synthesis of nanorod-aggregated functional hierarchical iron-containing MFI zeolite microspheres. *J. Mater. Chem A* **2015**, *3*, 14786–14793. [CrossRef]

23. Devaiah, D.; Smirniotis, P.G. Effects of the Ce and Cr Contents in Fe−Ce−Cr Ferrite Spinels on the High-Temperature Water−Gas Shift Reaction. *Ind. Eng. Chem. Res.* **2017**, *56*, 1772–1781. [CrossRef]

24. Damma, D.; Boningari, T.; Smirniotis, P.G. High-temperature water-gas shift over Fe/Ce/Co spinel catalysts: Study of the promotional effect of Ce and Co. *Mol. Catal.* **2018**, *451*, 20–32. [CrossRef]

25. Zhou, H.; Su, Y.; Liao, W.; Deng, W.; Zhong, F. Preparation, characterization, and properties of monolithic Fe/Al$_2$O$_3$/cordierite catalysts for NO reduction with C$_2$H$_6$. *Appl. Catal. A* **2015**, *505*, 402–409. [CrossRef]

26. Wei, Y.; Zhang, D.; Xu, L.; Chang, F.; He, Y.; Meng, S.; Su, B.L.; Liu, Z. Synthesis, characterization and catalytic performance of metal-incorporated SAPO-34 for chloromethane transformation to light olefins. *Catal. Today* **2008**, *131*, 262–269. [CrossRef]

27. Dědeček, J.; Čapek, L.; Kaucký, D.; SobalíK, Z.; Wichterlová, B. Siting and Distribution of the Co Ions in Beta Zeolite: A UV–Vis–NIR and FTIR Study. *J. Catal.* **2002**, *211*, 198–207. [CrossRef]

28. Čapek, L.; Kreibich, V.; Dědeček, J.; Grygar, T.; Wichterlová, B.; Sobalík, Z.; Martens, J.A.; Brosius, R.; Tokarová, V. Analysis of Fe species in zeolites by UV–VIS–NIR, IR spectra and voltammetry. Effect of preparation, Fe loading and zeolite type. *Microporous Mesoporous Mater.* **2005**, *78*, 279–289.

29. Schwidder, M.; Kumar, M.S.; Klementiev, K.; Pohl, M.M.; Brückner, A.; Grünert, W. Selective reduction of NO with Fe-ZSM-5 catalysts of low Fe content: I. Relations between active site structure and catalytic performance. *J. Catal.* **2005**, *231*, 314–330. [CrossRef]

30. Feng, X.; Cao, Y.; Lan, L.; Lin, C.; Li, Y.; Xu, H.; Gong, M.; Chen, Y. The promotional effect of Ce on CuFe/beta monolith catalyst for selective catalytic reduction of NO$_x$ by ammonia. *Chem. Eng. J.* **2016**, *302*, 697–706. [CrossRef]

31. Gao, F.; Walter, E.D.; Washton, N.M.; Szanyi, J.; Peden, C.H.F. Synthesis and evaluation of Cu/SAPO-34 catalysts for NH$_3$-SCR 2: Solid-state ion exchange and one-pot synthesis. *Appl. Catal. B* **2015**, *162*, 501–514. [CrossRef]

32. Imai, H.; Ogawa, T.; Sugimoto, K.; Kataoka, M.; Tanaka, Y.; Ono, T. Comparison of activities in selective catalytic reduction of NOx by C$_3$H$_8$ over Co/MFI, Fe/MFI, and H/MFI zeolite catalysts. *Appl. Catal. B* **2005**, *55*, 259–265. [CrossRef]

33. Zhang, R.; Shi, D.; Zhao, Y.; Chen, B.; Xue, J.; Liang, X.; Lei, Z. The reaction of NO+C$_3$H$_6$ +O$_2$ over the mesoporous SBA-15 supported transition metal catalysts. *Catal. Today* **2011**, *175*, 26–33. [CrossRef]

34. Nagayama, T.; Iizuka, H.; Katougi, K.; Mukai, T. Hydrocarbon Desorption Characteristics of Metal-impregnated Zeolite and Its Evaluation in Vehicle Test. *J. Jpn. Pet. Inst.* **2009**, *52*, 205–210. [CrossRef]

35. Kucherov, A.V.; Montreuil, C.N.; Kucherova, T.N.; Shelef, M. In situ high-temperature ESR characterization of FeZSM-5 and FeSAPO-34 catalysts in flowing mixtures of NO, C$_3$H$_6$, and O$_2$. *Catal. Lett.* **1998**, *56*, 173–181. [CrossRef]

36. Ma, Q.; Liu, Y.; He, H. Synergistic Effect between NO$_2$ and SO$_2$ in Their Adsorption and Reaction on γ-Alumina. *J. Phys. Chem. A* **2008**, *112*, 6630–6635. [CrossRef] [PubMed]

37. Satsuma, A.; Shimizu, K.I. In situ FT/IR study of selective catalytic reduction of NO over alumina-based catalysts. *Prog. Energy Combust. Sci.* **2003**, *29*, 71–84. [CrossRef]

38. Venkov, T.; Hadjiivanov, K.; Klissurski, D. IR spectroscopy study of NO adsorption and NO + O$_2$ co-adsorption on Al$_2$O$_3$. *Phys. Chem. Chem. Phys.* **2002**, *4*, 2443–2448. [CrossRef]

39. Wu, Z.; Jiang, B.; Liu, Y.; Haiqiang Wang, A.; Jin, R. DRIFT Study of Manganese/Titania-Based Catalysts for Low-Temperature Selective Catalytic Reduction of NO with NH$_3$. *Environ. Sci. Technol.* **2007**, *41*, 5812–5817. [CrossRef] [PubMed]

40. Long, R.; Yang, R. FTIR and kinetic studies of the mechanism of Fe^{3+}-exchanged TiO^{2-}pillared clay catalyst for selective catalytic reduction of NO with ammonia. *J. Catal.* **2000**, *190*, 22–31. [CrossRef]

41. Kumar, P.A.; Reddy, M.P.; Ju, L.K.; Hyun-Sook, B.; Phil, H.H. Low temperature propylene SCR of NO by copper alumina catalyst. *J. Mol. Catal. A* **2008**, *291*, 66–74. [CrossRef]

42. Long, J.; Zhang, Z.; Ding, Z.; Ruan, R.; Li, Z.; Wang, X. Infrared study of the NO reduction by hydrocarbons over iron sites with low nuclearity: Some new insight into the reaction pathway. *J. Phys. Chem. C* **2010**, *114*, 15713–15727. [CrossRef]

43. Jie, L.; Xinyong, L.; Qidong, Z.; Ce, H.; Dongke, Z. Insight into the mechanism of selective catalytic reduction of NO$_{(x)}$ by propene over the Cu/Ti$_{(0.7)}$Zr$_{(0.3)}$O$_2$ catalyst by Fourier transform infrared spectroscopy and density functional theory calculations. *Environ. Sci. Technol.* **2013**, *47*, 4528–4535.

44. Zhou, H.; Li, K.; Zhao, B.; Deng, W.; Su, Y.; Zhong, F. Surface properties and reactivity of Fe/Al$_2$O$_3$/cordierite catalysts for NO reduction by C$_2$H$_6$: Effects of calcination temperature. *Chem. Eng. J.* **2017**, *326*, 737–744. [CrossRef]

45. Kumar, M.S.; Schwidder, M.; Grünert, W.; Bentrup, U.; Brückner, A. Selective reduction of NO with Fe-ZSM-5 catalysts of low Fe content: Part II. Assessing the function of different Fe sites by spectroscopic in situ studies. *J. Catal.* **2006**, *239*, 173–186.

46. Zhou, H.; Su, Y.; Liao, W.; Deng, W.; Zhong, F. NO reduction by propane over monolithic cordierite-based Fe/Al$_2$O$_3$ catalyst: Reaction mechanism and effect of H$_2$O/SO$_2$. *Fuel* **2016**, *182*, 352–360. [CrossRef]

47. Liu, J.; Li, X.; Zhao, Q.; Zhang, D.; Ndokoye, P. The selective catalytic reduction of NO with propene over Cu-supported Ti–Ce mixed oxide catalysts: Promotional effect of ceria. *J. Mol. Catal. A Chem.* **2013**, *378*, 115–123. [CrossRef]

48. Yuan, D.; Li, X.; Zhao, Q.; Zhao, J.; Tadé, M.; Liu, S. A novel CuTi-containing catalyst derived from hydrotalcite-like compounds for selective catalytic reduction of NO with C$_3$H$_6$ under lean-burn conditions. *J. Catal.* **2014**, *309*, 268–279. [CrossRef]

49. Brandenberger, S.; Kröcher, O.; Wokaun, A.; Tissler, A.; Althoff, R. The role of Brønsted acidity in the selective catalytic reduction of NO with ammonia over Fe-ZSM-5. *J. Catal.* **2009**, *268*, 297–306. [CrossRef]